Runway foreign object detection using RGB

W. Chen
wishchen@buaa.edu.cn
Airport Research Institute
China Academy of Civil Aviation Science and Technology
Beijing
China

ABSTRACT

This paper presents an improved algorithm for foreign object debris (FOD) detection on the runway with several innovative techniques. The detection scheme incorporates four steps of geometric adjustment, background subtraction, clutter suppression and camouflage elimination. After geometric adjustment, the background model is built for each pixel with a set of RGB colour values taken in the past at the same location or in the neighborhood in the step of background subtraction. The background model samples are substituted randomly with an unfixed update period. Furthermore, the steps of clutter suppression and camouflage elimination are added to modify the segmentation map after background subtraction in order to increase the detection probability and decrease the false alarm rate. The overall algorithm is applied to the test data and real data on the runway. The results show that the RGB-based algorithm performs better than the classical gray-based techniques.

Paper No. 4124. Manuscript received 2 January 2014, revised version received 24 July 2014, accepted 4 September 2014.

https://doi.org/10.1017/S0001924000010356 Published online by Cambridge University Press

INTRODUCTION

Foreign object debris (FOD) at airports, including any substance, debris, or object in a location that can damage aircraft or equipment, can seriously threaten the safety of airport personnel and airline passengers, and can have a negative impact on airport logistics and operations[1]. Some typical FODs are illustrated in Table 1[1-3]. The most noted FOD related accident takes us back to 25 July 2000, where 100 passengers, nine crew members, and four people on the ground were killed when Air France Flight 4590 crashed after departing from Charles de Gaulle International Airport near Paris. The aircraft had run over a debris on the runway that had fallen from an aircraft that took off about four minutes earlier[2]. Internationally, FOD costs the aviation industry US$13 billion per year in direct plus indirect costs. The indirect costs are as much as ten times the direct cost value, representing delays, aircraft changes, incurred fuel costs, unscheduled maintenance, and the like. As part of the Federal Aviation Administration (FAA) Airport Safety Technology Research and Development Program, the University of Illinois, Center of Excellence for Airport Technology has been supporting the research and development activities of the FAA William J. Hughes Technical Center on FOD detection for more than ten years. The FAA initiated research to assess the four leading systems of FOD detection from QinetiQ, Stratech, Xsight Systems and Trex Enterprises during 2007 and 2008, and released the FAA Advisory Circular (AC) 150/5220-24 in 2009[3].

In China, several universities and research institutes also have been supporting the research on FOD detection techniques. Shanghai Jiao Tong University proposed a plan for runway security monitoring based on the review of current and proven state-of-the-art FOD detection systems[4]. Beijing Jiaotong University studied the techniques of image segmentation and noise suppression for FOD radar detection[5]. However, these researches merely focused on the theoretical algorithms but not the applicable techniques. China Academy of Civil Aviation Science and Technology (CAST),with the cooperation of Beihang University, developed a lost-cost video-based experimental system for airport runway security, called CAST FOD Detector. Following the preliminary system design experiences shared in Ref. 6, this paper mainly deals with the improvements on the FOD detection algorithm to obtain high detection rate and low false alarms. The remainder of this paper is organised as follows. Section 2 overviews the available techniques for FOD surveillance at airports. The improved FOD detection algorithm is discussed in Section 3. Compared with the original algorithm[6], the current algorithm makes a great progress in background subtraction and post-processing. Especially in the step of background subtraction, the RGB colour information of each pixel was used for the background modeling. In Section 4, experimental results against test data and real data collected on the runway show that our method outperforms the original algorithm. Section 5 concludes the paper.

2.0 SURVEY OF AVAILABLE TECHNIQUES FOR FOD DETECTION

Besides human observation, advanced technologies are now available for improved FOD detection, including capabilities for continuous monitoring on runways and other aircraft movement areas to supplement the capabilities of airport personnel. A summary of the system categories using different methods and sensors to perform the mission of detecting FOD has been given by FAA[3].

Human observation, which sets a bottom line for the performance of FOD detection systems, is the most traditional method. At present, airport personnel still serve as the primary tool for

https://doi.org/10.1017/S0001924000010356 Published online by Cambridge University Press

Table 1
Typical FODs[1-3]

Types	Examples
aircraft and engine fasteners	nuts, bolts, washers, safety wire
aircraft parts	fuel caps, landing gear fragments, oil sticks, metal sheets, trapdoors, tire fragments
flight line items	nails, personnel badges, pens, pencils, luggage tags, soda cans
apron items	paper and plastic debris from catering and freight pallets, luggage parts, and debris from ramp equipment
runway and taxiway materials	concrete and asphalt chunks, rubber joint materials, and paint chips
construction debris	pieces of wood, stones, fasteners and miscellaneous metal objects

FOD detection on runway surfaces, supporting regularly scheduled and special inspections. However, leaders of airports around the world have recognised that these manual means are not good enough as hundreds of FOD related events occur in the big airports every year, so more advanced devices are urgently needed.

Millimeter wave (MMW) radar is the earliest technical equipment as a supplement. 94·5GHz MMW radar has been used to continuously scan the designated pavement surfaces to detect FOD[7]. Generally, two or three units are located for each runway, 50m or more from the centre line. The system is able to detect a metallic cylindrical target measuring 3·0cm high and 3·8cm in diameter at ranges of up to 1km. The best advantage is its flexibility to day-night and all-weather conditions. MMW radar can also be mounted on top of a vehicle and scans the surface in front of the vehicle when moving. Such a system (78-81GHz) was developed by Trex Enterprises and operated at Chicago's Midway International Airport. Working staff staying on this mobile platform can remove the debris as soon as FOD is detected.

Optical camera is another popular means for FOD detection. Such system uses a high resolution camera that visually scans the runway surface. Generally, five to eight units are located for each runway, 150m or more from the centre line. Sophisticated image processing software is developed adapting to changing lighting and surface conditions. The system is able to detect a 2·0cm object target at ranges of up to 300m using only ambient lighting[3]. When FOD is found, the system provides an instant image of the debris, and then working staff is assigned immediately to remove it.

In recent years, there has been a trend to detect FOD with combined sensors to realise their advantages complement. Xsight Systems develops a system using a small hybrid unit that contains both 77GHz MMW radar and optical camera mounted next to the runway edge lights, covering an area of 1,500-3,500m^2. Exiting power for the edge light can be utilised to supply the system. Accordingly, an ideal location is chosen with low installation costs. Its high resolution (each pixel in the image represents 2mm of FOD) reduces the risk of generating false alarms[8].

Among the available techniques for FOD detection, the cost of optical camera is the lowest. In the coming section, we detail the video-based FOD detection algorithm based on RGB colours.

https://doi.org/10.1017/S0001924000010356 Published online by Cambridge University Press

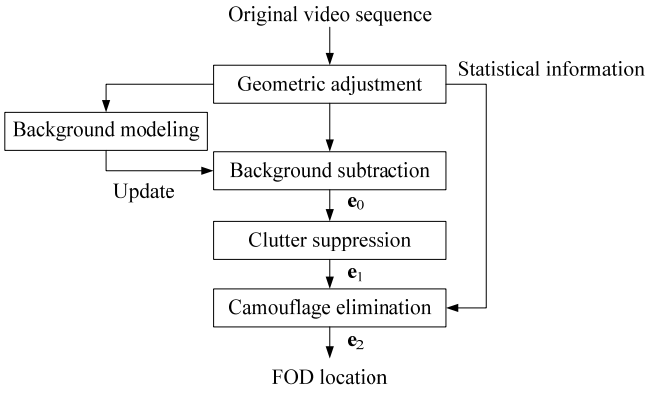


Figure 1. Flowchart of the FOD detection algorithm.

3.0 FOD DETECTION ALGORITHM BASED ON RGB COLOURS

As shown in Fig. 1, the flowchart of the FOD detection algorithm of the CAST FOD Detector is composed of geometric adjustment, background subtraction, clutter suppression and camouflage elimination. As the pre-processing before background subtraction, geometric adjustment is to use a series of mathematical models to reject the changes resulting from small camera motion when the surveillance area is relatively rigid. Many techniques have been proposed to remove these variations in many different forms. The general method is to align raw images from different sequences into the same co-ordinate system[9]. In Ref. 6, the background subtraction technique was based on the gray value of each pixel. However, in this paper, the background image is updated adaptively with some innovative techniques. The background model is built for each pixel with a set of RGB colour values taken in the past at the same location or in the neighborhood. In addition, the problems of clutter suppression and colour camouflage elimination are perfectly solved in post-processing as well. The segmentation maps obtained after these three steps are denoted by e_0, e_1 and e_2, respectively. We detail in the following the three processing steps.

3.1 Background subtraction with RGB colours

Most classical approaches and mainstream techniques to background subtraction rely on probability density functions (PDF) for every background pixel or at least the determination of statistical parameters, such as the mean or the variance. In fact, there is no imperative to compute the PDF as long as the goal of background subtraction is achieved. One alternative way is to build a model with real observed pixel values. The problem of background subtraction could be seen as a classification problem[10,11], and a new pixel value is classified with respect to its immediate neighborhood in the chosen colour space. Consequently, no estimation of the PDF of the background pixel is performed, and so the current value of the pixel is compared to its closest samples within the collection of samples. Each background pixel (x, y) is modeled by a collection of N background sample values

$$M[x, y] = \{\mathbf{v}_1, \mathbf{v}_2, ..., \mathbf{v}_N\} \quad \ldots (1)$$

https://doi.org/10.1017/S0001924000010356 Published online by Cambridge University Press

where v_i is the value in a given (r,g,b) colour space taken by the pixel located at (x,y) in the previous frames.

To classify a pixel value $v(x,y)$ according to its corresponding background model $M(x,y)$, we compare it to the centre of the model, which is computed as;

$$\mathbf{O}[x,y] = \frac{1}{N}\sum_{i=1}^{N}\mathbf{v}_i \quad \ldots (2)$$

The pixel value $v(x,y)$ is then classified as background if the Euclidean distance between the pixel and the centre of background model $M(x,y)$ is shorter than or equal to a given threshold θ. The distance is defined as;

$$d_0[x,y] = \left\|\mathbf{v}[x,y] - \mathbf{O}[x,y]\right\| \quad \ldots (3)$$

Thus, a binary segmentation image e_0 is obtained, where the target pixels are labelled as $e_0(x, y) = 1$ while the background pixels labelled as $e_0(x, y) = 0$.

To achieve accurate results over time, the background model must be continuously updated with each new frame. Our update method incorporates three important components: 1) a random update policy, which ensures a smooth decaying lifespan for the samples stored in the background pixel models, 2) a random time sub-sampling to extend the time windows covered by the background pixel models, and 3) a mechanism that propagates background pixel samples spatially to ensure spatial consistency and to allow the adaptation of the background pixel models that are masked by the foreground. These components are described in the following three subsections.

3.1.1 Random update policy

Many sample-based methods use first-in first-out policies to update their models[10]. However, from a theoretical point of view, a pixel model should contain samples from the recent past of the pixel but older samples should not necessarily be discarded. Instead of systematically removing the oldest sample from the pixel model, the sample is chosen to be discarded randomly according to a uniform probability density function.

Mathematically, the probability of a sample present in the model at time t being preserved after the update of the pixel model is given by $(N–1)/N$. Assuming after n times of updates, the probability decreases to

$$P(t,t+n) = \left(\frac{N-1}{N}\right)^n \quad \ldots (4)$$

This expression shows that the expected remaining lifespan of any sample value of the model decays exponentially. This random update policy contradicts the idea that older values should be replaced first.

3.1.2 Random time sub-sampling

The random update policy allows the background model to cover a large time window with a limited number of samples. In order to further extend the size of the time window covered by a background model of a fixed size, a random time sub-sampling strategy is proposed. The idea is that in many practical situations, it is not necessary to update each background pixel model for each

https://doi.org/10.1017/S0001924000010356 Published online by Cambridge University Press

new frame. In practice, when a pixel value has been classified as belonging to the background, a random process determines whether this value is used to update the corresponding sample. In our tests, the probability of being selected to update the background model is denoted by the parameter φ.

3.1.3 Spatial consistency through background samples propagation

Since some of the background pixels may be hidden by the foreground objects, a way should be provided to update these pixels of the background model. Note that the neighboring background pixels share a similar temporal distribution and that a new background sample of a pixel should also update the models of its neighboring pixels. According to this policy, background models hidden by the foreground will be updated with background samples from neighboring pixel locations from time to time.

More precisely, the set of background samples of a pixel (x, y), denoted as $M(x, y)$, could be updated with the values from the 4- or 8-connected spatial neighborhood of the pixel, that is $v(x, y) \in N_G(x, y)$, chosen at random according to a uniform law.

So far, the nature of the background subtraction algorithm with RGB colours has been detailed. In the coming section, we explain the post-processing steps of clutter suppression and camouflage elimination.

3.2 Clutter suppression

In spite of the background modeling with the RGB colours, there are still some false alarms across the segmentation image after background subtraction, so clutter suppression is applied on the foreground image to reject the false alarms.

Median filtering and morphological processing are two typical techniques for clutter suppression[6]. Although these methods can be effective in some cases, they suppress the false alarms at the cost of the detection rate. In this paper, a Markov random field (MRF) model is built in the neighborhood of the pixels labelled $e_0(x,y) = 1$ in the foreground image, where the target association probabilities are calculated to modify the initial segmentation map e_0. The probability is calculated as

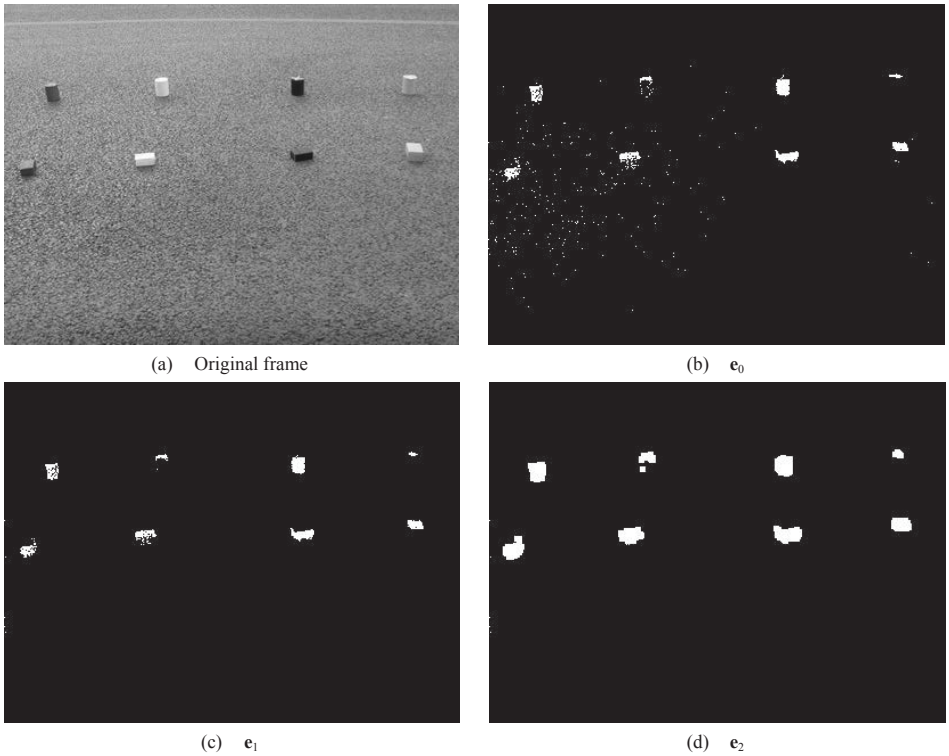
$$P_T\left(\mathbf{I}[x,y] \middle| \mathbf{e}_0[x,y]=1\right) = \frac{N\left(E=\mathbf{e}_0^T\right)}{N\left(E=\mathbf{e}_0^B\right)} \quad \ldots (5)$$

where E is the MRF model, e_0^B denotes the label field around when $e_0(x, y) = 0$ and e_0^T denotes the case when $e_0(x,y) = 1$. In this paper, the MRF model is a square window with the width of l. According to formula[5], the target pixels in e_0 are then classified as false alarms in the new modified segmentation map e_1 if their corresponding target association probabilities are less than or equal to a given threshold γ. Obviously, in case that a pixel labelled as target in e_0 is mainly surrounded by target pixels (e_0^T), its target association probability is higher, and is more likely to be retained as a target pixel in the new binary image e_1. Similarly, if the target pixel in e_0 is mainly surrounded by background pixels (e_0^B), its target association probability is lower, and is more likely to be rejected as a false alarm in the new segmentation map e_1.

3.3 Camouflage elimination

In some cases, the FOD target is difficult to detect and usually missing due to its high colour similarity with the background. Since the target is usually a smooth and connected region in the image, the segmentation map e_1 should be further processed to eliminate the target camouflage based on the RGB statistics from the original image. The neighboring pixels of the target pixels in

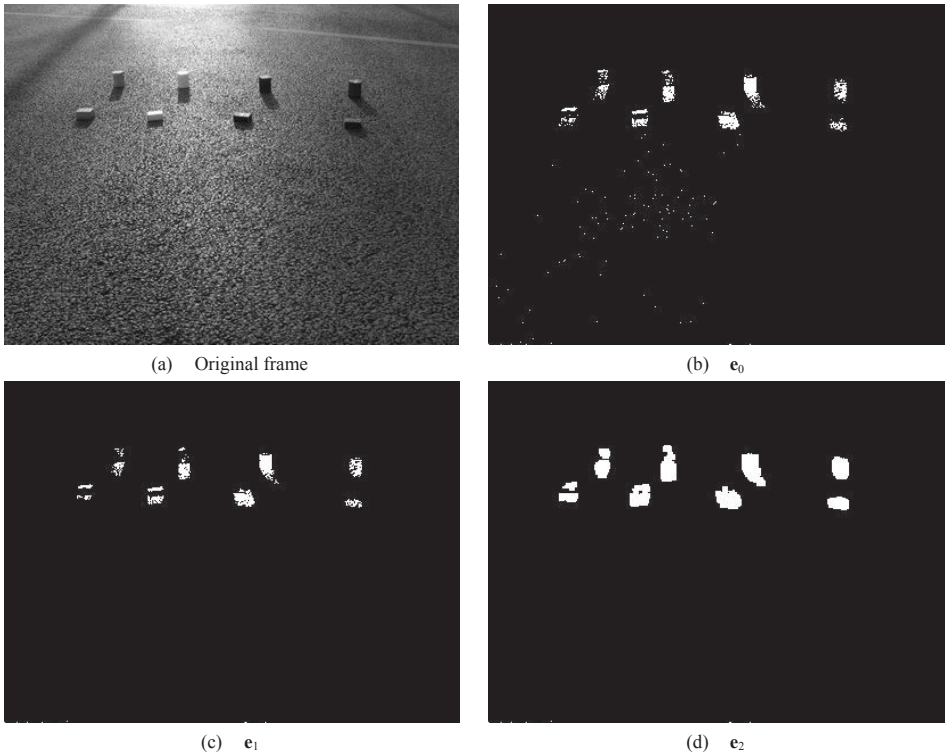
https://doi.org/10.1017/S0001924000010356 Published online by Cambridge University Press



(a) Original frame (b) $\mathbf{e}_0$

(c) $\mathbf{e}_1$ (d) $\mathbf{e}_2$

Figure 2. Detection results for FOD in the shadow.



(a) Original frame (b) $\mathbf{e}_0$

(c) $\mathbf{e}_1$ (d) $\mathbf{e}_2$

Figure 3. Detection results for FOD in the sunshine.

https://doi.org/10.1017/S0001924000010356 Published online by Cambridge University Press

e_1, denoted as e_1^T, are possible camouflage pixels, which may resume to be labelled as target in e_2. The mean Euclidean distance between the candidate camouflage pixels and the target pixel in e_1 is:

$$d_{\mathrm{T}}\left(\mathbf{v}[x,y]\right)=\frac{1}{|\mathrm{S}|}\sum_{[x,y]\in \mathrm{S}}\left\|\mathbf{v}[x,y]-\mathbf{v}[x_0,y_0]\right\| \quad \ldots (6)$$

where S denotes the neighborhood window around (x_0, y_0) in the original image with the width of l. The pixel (x_0, y_0) is detected as target in e_1. |S| represents the number of neighboring pixels. It reveals in Ref. 6 that the detected probability of the neighborhood pixels depend on their mean distance to the pixel (x_0, y_0). The neighboring pixels will resume to be labelled as target in e_2 if the distance is shorter than or equal to a given threshold η.

After the above three steps, the connected regions labelled with $e_2(x, y) = 1$ in the final segmentation image are defined as FOD targets and their centres are extracted.

4.0 EXPERIMENTAL RESULT ANALYSIS

The proposed algorithm was applied on the test data and real data collected at airports. Our experimental system was temporarily settled on the grassland besides the runway to obtain some original data[6]. Compared with the detection results of the traditional algorithm, the performance of the proposed algorithm was accessed through the probability of detection (P_d) and false alarms (P_{fa}).

Assuming that in a detected image the number of true target pixels is A and the number of true background pixels is B, and T pixels among the target pixels are correctly detected as targets, and F pixels from the background pixels are incorrectly classified as targets. So, the values of P_d and P_{fa} are defined as;

$$P_{\mathrm{d}}=\frac{T}{A},\quad P_{\mathrm{fa}}=\frac{F}{B}. \quad \ldots (7)$$

An effective target detection algorithm should increase the value of P_d and keep the value of P_{fa} at the lower level as well. In this paper, the number of target pixels and background pixels were manually classified and counted. The number of correctly extracted target centres is the number of detected targets, denoted by a, while those extracted by error represents the number of false alarms, denoted by b.

4.1 Test data

The proposed algorithm was applied on two sets of test images under different illuminations. The data was collected with FOD targets with different shades (white, light-grey, dark-grey and black) on the asphalt pavement. The test images in the experiments were 480 × 640 pixels in wide and 8-bit gray levels in the (r, g, b) colour space.

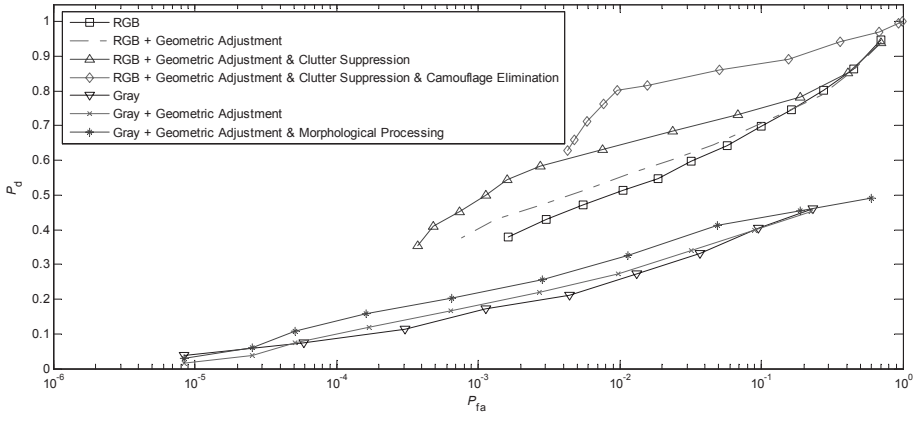
Fig. 2 shows the overall process for FOD detection in the shadow. Eight FOD targets, four cylinders and four cubes, were added to the asphalt pavement. Fig. 2(a) is the original frame, where colours of different sides of each target vary according to different illumination angles. The number of samples in the background model is set to $N = 10$. Fig. 2(b) shows the initial segmentation image e_0, where the background is subtracted but a number of false alarms remain and most parts of some FODs are missing due to its high similarity with the background. The optimal threshold in this step was set to $d_0 = 100$. After clutter suppression, all false alarms composed of only a few pixels are rejected, and the result e_1 is shown in Fig. 2(c). The threshold in this step was set

https://doi.org/10.1017/S0001924000010356 Published online by Cambridge University Press

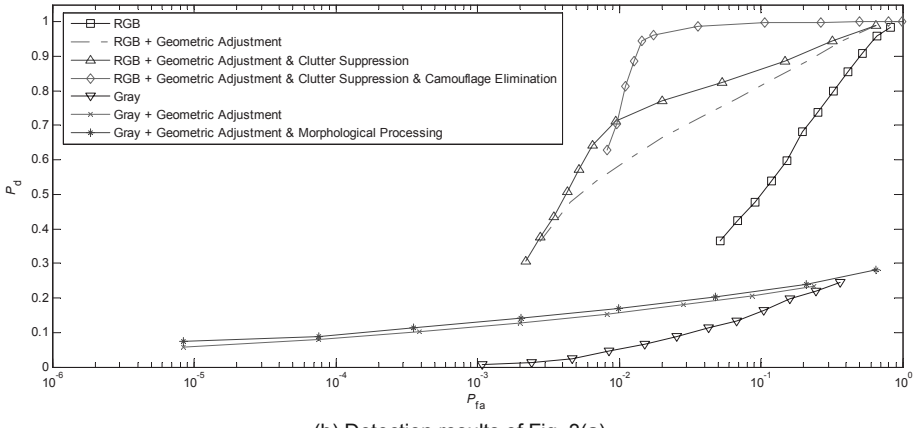
Table 2
Quantitative segmentation results

Segmentation results	Fig. 2		Fig. 3	
	P_d	P_{fa}	P_d	P_{fa}
e_0	0.473	0.002	0.478	0.005
e_1	0.453	0.001	0.435	0.003
e_2	0.712	0.006	0.814	0.011

to $\gamma = 0{\cdot}15$ and the window size was $l = 5$. The MRF approach outperforms the morphological methods in reducing the false alarms without influence on already detected regions. To eliminate the camouflage effects and improve the detection performance, detected probability of neighborhood pixels around the target-labelled pixel is calculated using the statistical information from the original frame. The threshold was set to $\eta = 50$ in this step. The window size was also set at $l = 5$. The gaps inside the targets are converged and the boundaries grow to certain extent in Fig. 2(d).



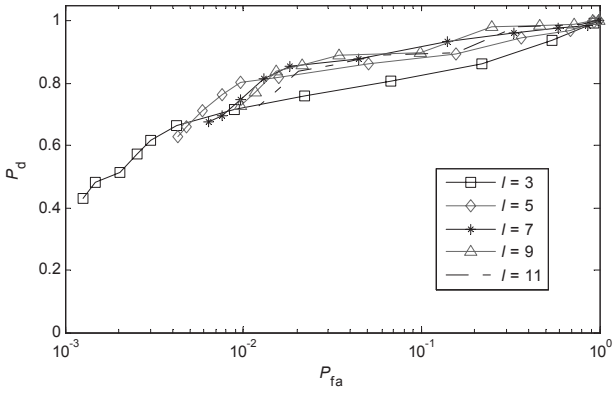
(a) Detection results of Fig. 2(a)



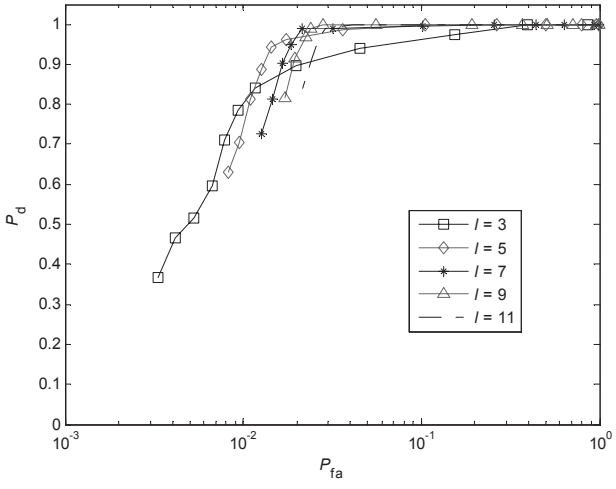
(b) Detection results of Fig. 3(a)

Figure 4. ROC curves of seven FOD detection techniques.

https://doi.org/10.1017/S0001924000010356 Published online by Cambridge University Press



(a) Detection results of Fig. 2(a)



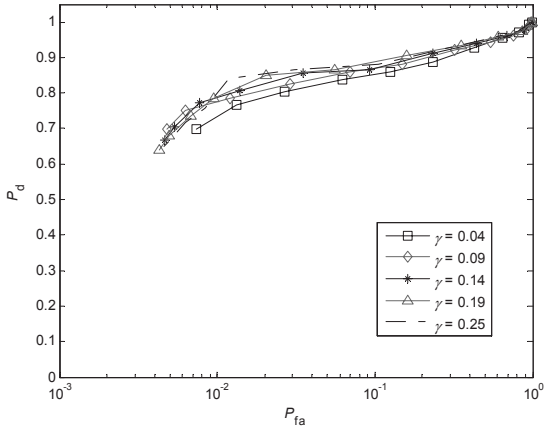
(b) Detection results of Fig. 3(a)

Figure 5. Influence of the value of l on the ROC curves.

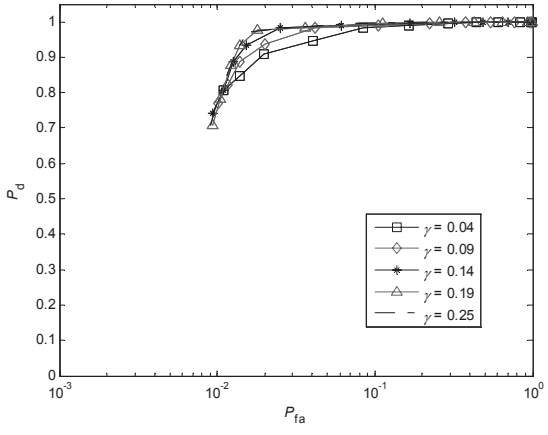
Figure 3 shows the overall process for FOD detection in the sunshine coming from behind the targets. The parameters were the same with those set for Fig. 2. Fig. 3(a) is the original frame. The detection of shadows is a source of confusion for subsequent processing. However, it is tolerable for engineering application because the shadow is always connected to the object. Fig. 3(b) shows the initial segmentation map e_0. (c) and (d) of Fig. 3 are e_1 and e_2, the segmentation results after clutter suppression and camouflage elimination. The shadows of targets are also segmented as targets, seriously affecting the detection results. In fact, the interference of shadows reduces the difficulty of FOD detection, which can be utilised in engineering application.

Table 2 reveals the quantitative segmentation results of Fig. 2 and Fig. 3 in the terms of P_d and P_{fa}. It is clear that clutter suppression reduce the false alarm rate at the cost of reducing the detection rate, and camouflage elimination increase the detection rate at the cost of increasing the false alarm rate. The data provided in Table 2 also shows that the false alarm rate of the detection results of Fig. 3 is relatively higher than that of Fig. 2 due to the influence of sunshine.

https://doi.org/10.1017/S0001924000010356 Published online by Cambridge University Press



(a) Detection results of Fig. 2(a)



(b) Detection results of Fig. 3(a)

Figure 6. Influence of the value of γ on the ROC curves.

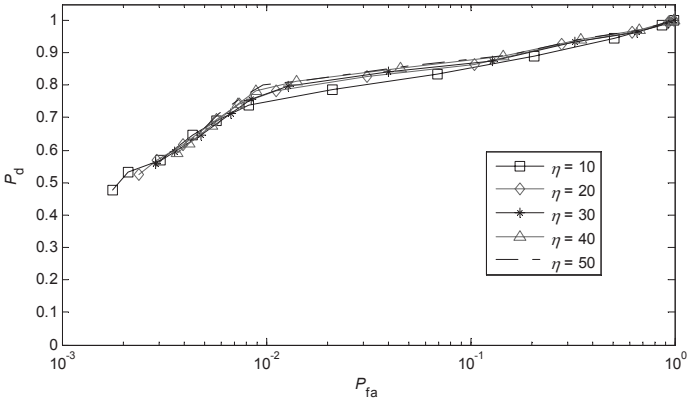
Figure 4 shows the receiver operator characteristic (ROC) curves of seven comparison algorithms. The algorithm proposed herein using the RGB colour space is called RGB and that proposed in Ref. 6 using the gray space is called Gray. Obviously, the RBG-based algorithms greatly outperform the Gray-based algorithms in detection results. Moreover, the combination of RGB subtraction, clutter suppression and camouflage elimination performs better than the Gray-based algorithm proposed in Ref. 6 where morphological processing is used for clutter rejection. Compared with Fig. 4(a), the false alarm rate of Fig. 4(b) is totally higher when the detection probability is close to 100%, which is mainly caused by the target shadow. As for the influence of geometric adjustment, clutter suppression and camouflage elimination, these techniques are more effective to Fig. 3(a) than to Fig. 2(a).

Figure 5 shows the influence of the value of window size l to the detection results. Note that this parameter was set at the same value both in the step of clutter suppression and camouflage elimination. It is revealed in Fig. 5 that the ROC curves almost overlap with each other when l

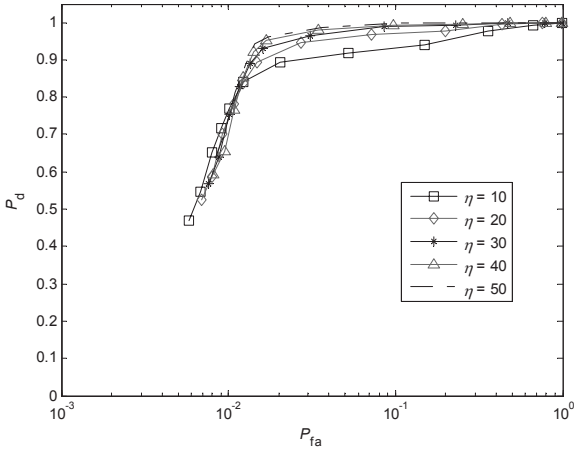
https://doi.org/10.1017/S0001924000010356 Published online by Cambridge University Press

Table 3
Quantitative detection results of real data at Nanyang Airport

θ	The algorithm in Ref. 6		The proposed algorithm	
	a	*b*	*a*	*b*
95	5	5	5	12
100	4	4	5	6
110	3	3	5	3
112	3	1	5	0
114	3	1	5	0
116	3	1	4	0
118	3	0	4	0
120	3	0	4	0
130	3	0	4	0



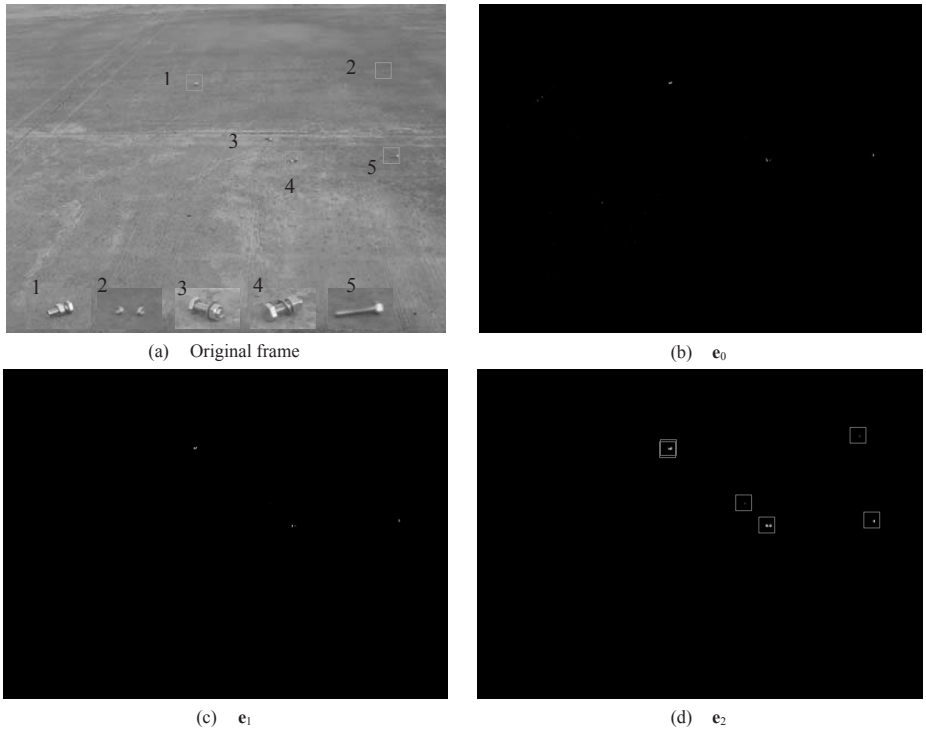
(a) Detection results of Fig. 2(a)



(b) Detection results of Fig. 3(a)

Figure 7. Influence of the value of η on the ROC curves.

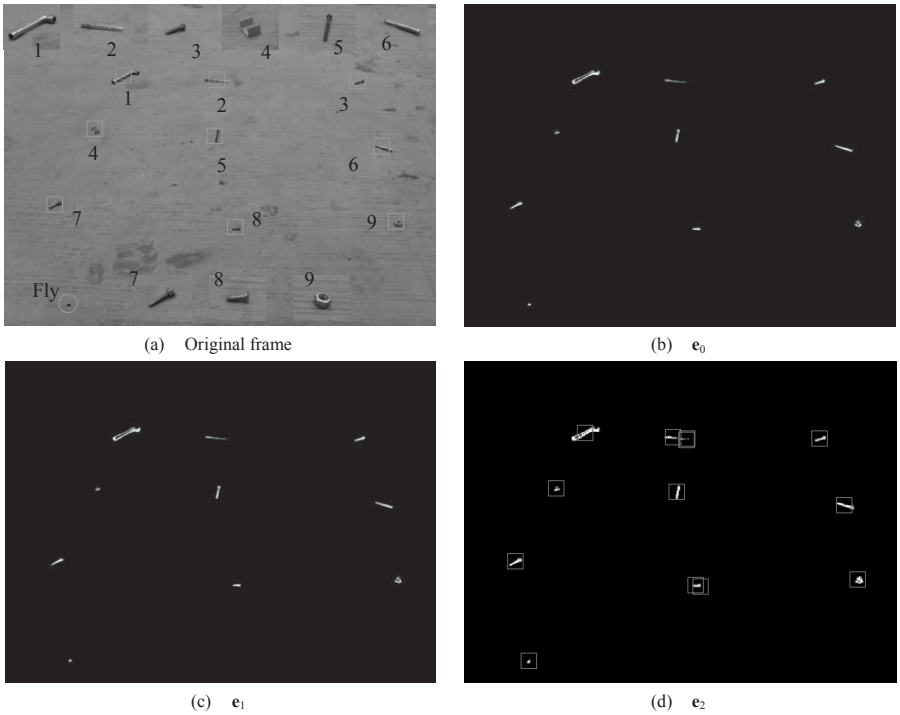
https://doi.org/10.1017/S0001924000010356 Published online by Cambridge University Press



(a) Original frame (b) $\mathbf{e}_0$

(c) $\mathbf{e}_1$ (d) $\mathbf{e}_2$

Figure 8. Detection results of real data at Nanyang Airport.



(a) Original frame (b) $\mathbf{e}_0$

(c) $\mathbf{e}_1$ (d) $\mathbf{e}_2$

Figure 9. Detection results of real data at Beihai Airport.

https://doi.org/10.1017/S0001924000010356 Published online by Cambridge University Press

is set to 5, 7, 9 and 11. Thus, to reduce the computation load, the parameter should be set to l = 5 as the above.

Figure 6 shows the influence of the value of γ in the step of clutter suppression to the detection results. It is clear that the ROC curves stay almost unchanged when γ is set to 0·09, 0·14, 0·19 and 0·25. Therefore, it is approved that the clutter left in the foreground image usually includes a small quantity of pixels.

Figure 7 shows the influence of the value of η in the step of camouflage elimination to the detection results. It is revealed that the ROC curves keep almost unchanged when η is set to 20, 30, 40 and 50. It is demonstrated that the Euclidean distance between most of the neighboring camouflage pixels and the target pixel in the e_1 are less than 20.

4.2 Real data on the runway

The proposed algorithm was also applied to two image sequences collected at Nanyang Airport, Henan Province and Beihai Airport, Guangxi Province, respectively. The real images in the experiments were 2,304 × 3,072 pixels in wide.

Figure 8 shows the detection results of a frame collected at Nanyang Airport in the morning with gentle light. As shown in Fig. 8(a), five FOD targets were placed on the runway. Target 1, 3, 4 were silver-colour screw bolts with caps, approximately 3cm in length; target 2 was two silver-colour screw caps; target 5 was a yellow screw bolt, approximately 5cm in length. In the terms of a and b, Table 3 illustrates the detection results of the new algorithm and that proposed in Ref. 6. The proposed algorithm could detect all the five targets with zero false alarm when the threshold was set to θ = 112 or 114. The optimal detection results after background subtraction and clutter suppression are shown in Fig. 8(b) and Fig. 8(c). In Fig. 8(d), the five target centres are plotted correctly after camouflage elimination. However, the algorithm proposed in Ref. 6 could detect all the five targets at the cost of five false alarms (θ = 95).

Figure 9 shows the detection results of a frame collected at Beihai Airport at dawn. As shown in Fig. 9(a), nine FOD targets were placed on the runway, including a wrench, some screws, metal debris, and nails. All the nine targets are detected by the proposed algorithm with no false alarms. Otherwise, a fly is also detected at the lower left corner of the image.

It is clear that θ has a large impact on the probabilities of detections and false alarms. As the value of θ increases, the probability of false alarms decreases at the cost of the probabilities of detections. Therefore, the value of θ should be set carefully to achieve the balance between these two parameters.

4.3 Limitations of the algorithm

A potential problem is that the CAST FOD Detector using the proposed algorithm could not be used in inclement weather due to the strong interference, which is a common limitation of the video-based FOD detection systems. Since the MMW radar is less interfered by the inclement weather, the combination of MMW radar and optimal camera could provide a possible solution.

5.0 CONCLUSION

In this paper, we introduced a FOD detection algorithm specially designed for the runway surveillance from a static camera located beside the runway. The proposed algorithm is based on background subtraction with the RGB colours, greatly improving the detection results of the Gray-based algorithm proposed in Ref. 6. The background model is updated periodically with

https://doi.org/10.1017/S0001924000010356 Published online by Cambridge University Press

environment changes. A new update mechanism is proposed to replace the background model samples randomly with an unfixed update period. This results in the longer lifespan for each model sample, broadening the length of the time window covered by the pixel model and reducing the required number of samples needed for each pixel. Furthermore, the neighboring background pixels are also allowed to update the background model. After the RGB-based background subtraction, the post-processing of clutter suppression and camouflage elimination is added to improve the segmentation results. Finally, the detection results of the RGB-based algorithms were compared with those with the Gray-based algorithms against test data and real data. The RGB-based algorithm combined with the post-processing is shown to outperform all of these algorithms.

ACKNOWLEDGEMENTS

This work is jointly funded by the National Natural Science Foundation of China (NSFC) and Civil Aviation Administration of China (CAAC) (No. 61001134).

REFERENCES

1. NAS-412: Foreign Object Damage/Foreign Object Debris (FOD) Prevention. Aerospace Industries Association – National Aerospace Standard, 1 October 1997.
2. Patterson, J. Jr. Foreign Object Debris (FOD) detection research. International Airport Review, 2008, **11**, (2), pp 22-27.
3. O'DONNELL, M.J. Airport Foreign Object Debris (FOD) Detection Equipment. FAA, AC No: 150/5220-24, 2009.
4. YU, L. and GANG, X. Study and design on FOD detection and surveillance system for airport runway, *Laser & Infrared*, 2011, **41**, (8), pp 909-915.
5. MANJIE, F. Airport FOD detection research on runway. Beijing Jiaotong University, China, 2011.
6. QUNYU, X., HUANSHENG, N., and WEISHI, C. Video-based foreign object debris detection. IEEE International Workshop on Imaging Systems and Techniques Proceedings, pp 123-126, 11-12 May, 2009.
7. BEASLEY P.D.L., BINNS G. and HODGES R.D., *ET AL*. Tarsier®, a millimeter wave radar for airport runway debris detection. Radar Conference, 2004, pp 261-264.
8. VOGEL, B. An object lesson in finding FOD. Jane's Airport Review, 2008, **20**, (8), pp 56-57.
9. RADKE R.J., ANDRA S. and AL-KOFAHI O., *et al* Image change detection algorithm: a systematic survey. IEEE Transactions on Image Processing, 2005, **14**, (3), pp 294-307.
10 BARNICH, O. and VAN DROOGENBROECK M. ViBe: A Universal Background Subtraction Algorithm for Video Sequences. IEEE Trans. Image Processing, 2011, **20**, (6), pp 1709-1724.
11 MCHUGH, J., KONRAD, J. and SALIGRAMA, V. *et al* Foreground-Adaptive Background Subtraction. IEEE Signal Processing Letters, 2009, **16**, (5), pp 390-393.

https://doi.org/10.1017/S0001924000010356 Published online by Cambridge University Press